Variability of Cosmogenic ^{35}S in Rain—Resulting Implications for the Use of Radiosulfur as Natural Groundwater Residence Time Tracer

Michael Schubert [1,*], Kay Knöller [2], Ina Tegen [3] and Lucrezia Terzi [4]

[1] Helmholtz Centre for Environmental Research, Permoserstr. 15, 04318 Leipzig, Germany
[2] Helmholtz Centre for Environmental Research, Theodor-Lieser-Str. 4, 06120 Halle, Germany; kay.knoeller@ufz.de
[3] Leibniz Institute for Tropospheric Research, Permoserstr. 15, 04318 Leipzig, Germany; itegen@tropos.de
[4] Belgian Nuclear Research Centre SCK-CEN, Boeretang 200, 2400 Mol, Belgium; lucrezia.terzi@sckcen.be
[*] Correspondence: michael.schubert@ufz.de

check for updates

Abstract: Information about groundwater residence times is essential for sustainable groundwater management. Naturally occurring radionuclides are suitable tools for related investigations. While the applicability of several long-lived radionuclides has been demonstrated for the investigation of long residence times (i.e., years, decades, centuries and more), studies that focus on sub-yearly residence times are only scarcely discussed in the literature. This shortage is mainly due to the rather small number of radionuclides that are generally suitable for the purpose and show at the same time adequately short half-lives. A promising innovative approach in this regard applies cosmogenic radiosulfur (^{35}S). ^{35}S is continuously produced in the stratosphere from where it is conveyed to the troposphere or lower atmosphere and finally transferred with the rain to the groundwater. As soon as the meteoric water enters the subsurface, its ^{35}S activity decreases with an 87.4 day half-life, making ^{35}S a suitable time tracer for investigating sub-yearly groundwater ages. However, since precipitation shows a varying ^{35}S activity during the year, setting up a reliable ^{35}S input function is required for sound data evaluation. That calls for (i) an investigation of the long-term variation of the ^{35}S activity in the rain, (ii) the identification of the associated drivers and (iii) an approach for setting up a ^{35}S input function based on easily attainable proxies. The paper discusses ^{35}S activities in the rain recorded over a 12-month period, identifies natural and anthropogenic influences, and suggests an approach for setting up a ^{35}S input function applying ^{7}Be as a proxy.

Keywords: ^{35}S; ^{7}Be; groundwater residence time; tracer; input function

1. Introduction

The knowledge of groundwater residence times is essential for the sustainable management of groundwater resources. This general fact can be underpinned with three specific aspects: (i) the vulnerability of an aquifer (regarding anthropogenic contamination) depends largely on the travel time needed by the meteoric water to cross the unsaturated soil zone covering the groundwater body. (ii) Sustainable groundwater abstraction management is mainly based on groundwater residence time evaluation. (iii) Groundwater residence time information is essential for evaluating groundwater migration patterns and the associated matter (and contaminant) transport.

Commonly, the investigation of groundwater residence times relies on field surveys that apply environmental tracers, i.e., tracers that occur naturally in the groundwater. Suitable in this regard are components that meet two general requirements: (i) their concentration in groundwater changes as

a function of time and (ii) they enter the subsurface (dissolved in the meteoric water or any surface water) either with a time-constant concentration or with a specific time-variant input function.

Powerful residence time tracers include (besides stable isotopes such as ^{40}Ar, ^{3}He, δ^{2}H, or δ^{18}O) a range of ubiquitously occurring radionuclides. A key criterion for selecting site-specifically the most suitable radionuclide is its half-life, which should be in the same range as the groundwater residence time expected for the investigated aquifer domain. Rather long-lived radionuclides (such as ^{3}H, ^{14}C, ^{36}Cl, ^{39}Ar, ^{81}Kr, and ^{85}Kr) are generally suitable for investigating high groundwater ages (Figure 1) and a great number of studies that aimed at investigating aquifer systems with water residence times between 10 and 10^{6} years have been published. In contrast, radiotracer-based investigations that focus on sub-yearly groundwater residence times are scarcely discussed in the literature. This is because only a limited number of ubiquitously occurring radionuclides show a half-life short enough for covering the sub-yearly timeframe. Examples of suitable short-lived radionuclides are the frequently applied ^{222}Rn (e.g., [1–3]) or the radium species ^{224}Ra and ^{223}Ra (e.g., [4,5]).
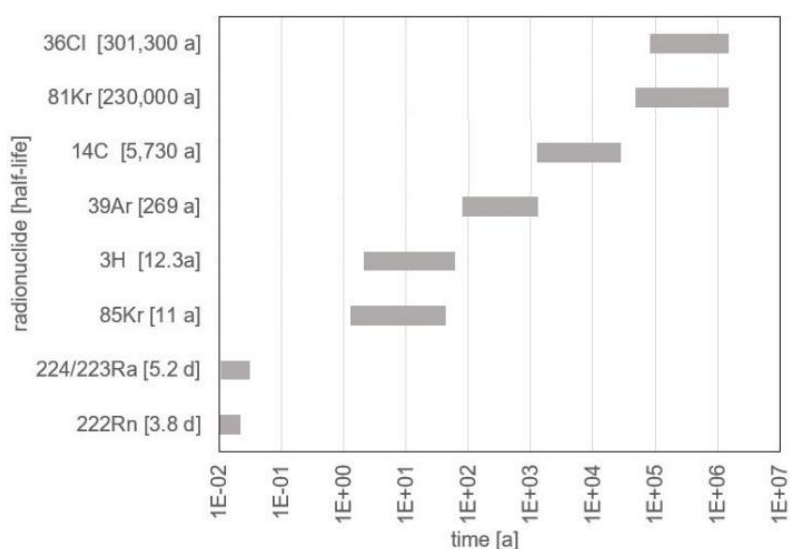

Figure 1. Naturally occurring radionuclides that are conventionally applied as aqueous residence time tracers plotted versus approximately covered residence time ranges.

The state-of-the-art situation is generally illustrated in Figure 1. The image reveals that the timeframe between about 1 and 12 months is not satisfactorily covered by the radioactive residence time tracers that are conventionally applied.

A potential candidate to fill this gap is the naturally occurring radioisotope beryllium-7 (^{7}Be). It shows a half-life of 53.3 days and is hence (at least in this regard) suitable for investigating groundwater residence times of up to about eight months. ^{7}Be is produced through cosmic ray spallation of mainly oxygen and nitrogen within the upper troposphere and lower stratosphere (UTLS zone) [6–8]. There it attaches to aerosols, which are washed out by (dry deposition and) mainly precipitation [9,10]. Since no natural ^{7}Be sources exist in the subsurface, the ^{7}Be activity concentration of the meteoric water declines once it enters the ground. However, ^{7}Be has a high tendency to sorb not only to aerosols in the upper atmosphere but also to the soil matrix. Thus, a substantial and nonquantifiable share of the dissolved beryllium is retarded by the soil matrix [11,12], which (in contrast to its applicability as a tracer for atmospheric dynamics, [10,13]) impedes its applicability as a quantitative aqueous tracer in groundwater.

A promising alternative approach for covering sub-yearly groundwater residence times is based on the application of naturally occurring radioactive sulfur as aqueous tracer ("radiosulfur"; ^{35}S, [14]). Comparable to ^{7}Be, the radionuclide is continuously produced by cosmic ray spallation (of ^{40}Ar) in the stratosphere where it rapidly (ca. one second) oxidizes to sulphate. Due to its short half-life of

87.4 days, some of the produced ^{35}S decays to ^{35}Cl during stratosphere/troposphere air exchange. Still, most ^{35}SO$_4^{2-}$ gets dissolved in meteoric water and is transferred as precipitation to the earth's surface and finally to the groundwater [15].

^{35}SO$_4^{2-}$ activities in rain range generally between about 10 and 150 mBq/L ([16–19]; own measurements). As soon as the ^{35}S containing meteoric water (C_0) enters the subsurface, ^{35}S decay is not supported by ^{35}S production anymore, which makes the decline of the initial ^{35}S activity concentration in the groundwater (C_t) an indicator for its residence time (t) in the ground (determined by the ^{35}S decay constant λ) (Equation (1)).

$$C_t = C_0 e^{-\lambda t} \tag{1}$$

In contrast to ^{7}Be, sulphate ^{35}SO$_4^{2-}$ is not retarded by the soil or aquifer matrix. This makes radiosulfur a residence time tracer suitable for groundwater ages between about three and nine months (i.e., between one and three ^{35}S half-lives, [20–22]).

Still, scanning the literature reveals that only a few related case studies have been published so far. These studies are generally limited to high geographical elevations, where snowmelt is the dominant hydrological recharge event. This boundary condition limits ^{35}S input into the groundwater to the peak snowmelt, i.e., it simplifies the ^{35}S input to a distinct value [20,21,23,24]. This neglects the fact that ^{35}S is likely to show considerable variability in the rain over the course of a year (e.g., [25,26]).

This variability is mainly due to large-scale atmospheric circulation dynamics, i.e., due to stratosphere/troposphere air mass exchange and convective tropospheric air circulation, which are, to a large degree, bound to seasonal patterns in atmospheric processes [10]. Besides such temporal variations, significant latitudinal variations of ^{35}S in the atmosphere and the rain are also likely. The varying deflection of cosmic rays causes this lateral variability due to the Earth's magnetic field's increased strength closer to the equator [10]. Another influential factor for ^{35}S variability in the rain is the rainfall dynamics, i.e., sulphate washout by precipitation [27,28].

The resulting regional and seasonal variability of ^{35}S in the rain suggest that the experiences reported for the use of ^{35}S as aqueous residence time tracer in alpine/subalpine watersheds are of only limited use in moderate climates. That implies that the variability of the ^{35}S activity in the rain (and the associated drivers) needs to be investigated and understood more comprehensively. Setting up region-specific long-term ^{35}S input functions is mandatory. Understanding the challenges related to this requirement calls for (i) an exemplary systematic long-term investigation of the ^{35}S activity in the rain in a certain study region, (ii) the identification of the drivers of the temporal long-term ^{35}S variability and (iii) the suggestion of an easily attainable ^{35}S proxy that can be applied for supporting the setup of a regional ^{35}S input function (the latter is desirable because long-term ^{35}S datasets are hardly ever available and ^{35}S in water analysis is rather laborious).

The presented paper discusses ^{35}S activities in the rain recorded over a 12-month period at a distinct location in Germany and suggests an approach regarding the setup of a regional ^{35}S input function. The approach applies ^{7}Be in atmospheric air as ^{35}S proxy. Furthermore, the results are backed and evaluated based on the time series of the aerosol optical depth (AOD) and the activity concentration of naturally occurring ^{212}Pb in atmospheric air.

2. Materials and Methods

2.1. Radiosulfur Sampling and Measurement

All ^{35}S data of the study was attained in a sampling campaign that aimed at collecting samples from as many major rain events as possible over the course of 12 months (August 2019–July 2020). A sampling station was installed, uncovered by trees, in a rural environment close to the city of Leipzig, Germany. The area is located at an elevation of 155 masl, characterized by an average annual rainfall of 550 mm, and an average annual temperature of 11 °C.

All rain samples were collected from a 31 m^2 inclined laminated rain collector plane via a downpipe into a 200-litre HDPE container. Hence, all rain events of up to 6.5 mm precipitation (88% of the 60 sampled rain events) were quantitatively collected. The container was isolated from any other environmental depositions besides rain. The rain collector surface, the downpipe and the container were cleaned regularly, during autumn (leaves) and springtime (pollen) and after storm events.

All related meteorological data was recorded at a professional meteorological station located only 3 km from the rain sampling location. Hence, all samples could be associated with specific rain events and their intensity.

Each rain sample was representatively transferred from the 200-litre sample container into a 20-litre plastic canister. Since no elevated sulphate concentrations were expected in the samples [29], all sample processing and measurement followed the suggestions for low-sulphate sample preparation for liquid scintillation counting (LSC) given by [30]. A Quantulus GCT 6220 liquid scintillation counter was used for all ^{35}S activity measurements. To allow reasonable statistical reliability of the counting results (counting error < 1%), each measurement lasted 24 h. The detection background was counted and subtracted from the sample counts by measuring a ^{35}S-dead (and ^{3}H-dead) background vial before each measurement. To optimize the signal-to-noise-ratio of the measurement results, the specific LSC detection options were set as given in Table 1.

Table 1. Quantulus GCT 6220 settings for counting ^{35}S in aqueous solution with Hionic-Fluor.

Parameter	Setting
Assay type	DPM (single)
Quench indicator	tSIE/AEC
2 Sigma threshold	0.5%
Counting energy window	3–167 keV
Coincidence time	18 ns
Delay before burst	75 ns

2.2. Using Atmospheric ^{7}Be as ^{35}S Proxy

In Central Europe we usually observe increased activity concentrations of ^{7}Be in the lower atmosphere during the warm and dry summer season. The main reasons for this annual pattern are the following.

(i) The tropopause, i.e., the boundary layer between the stratosphere and troposphere rises during the warm season. This upward shift increases the import of ^{7}Be from the UTLS zone to the lower atmosphere [13,31].

(ii) The zone between the two latitudinal circulation features the Hadley Cell (in the northern hemisphere in the south) and the Ferrel Cell (in the north) is called the Hadley Ferrel Divergence Zone (HFDZ). Within the HFDZ air masses are continuously conveyed from the upper part to the lower part of the troposphere (Figure 2) [32]. While (in the northern hemisphere) the HFDZ is generally active at a latitude of about 30° north it migrates, with the start of the warm season, northward and approaches Central Europe annually during the summer.

As discussed in Section 1, both ^{7}Be and ^{35}S are primarily created in the lower stratosphere both triggered by cosmic ray spallation. It can hence be assumed that their production rates correlate. Furthermore, both nuclides are conveyed by the same abovementioned large-scale atmospheric processes to the troposphere and lower atmosphere as illustrated in Figure 2. Hence, it was postulated that exceptionally high (or low) ^{7}Be activities in the lower atmosphere indicate the simultaneous presence of exceptionally high (or low) ^{35}S activities in the rain.
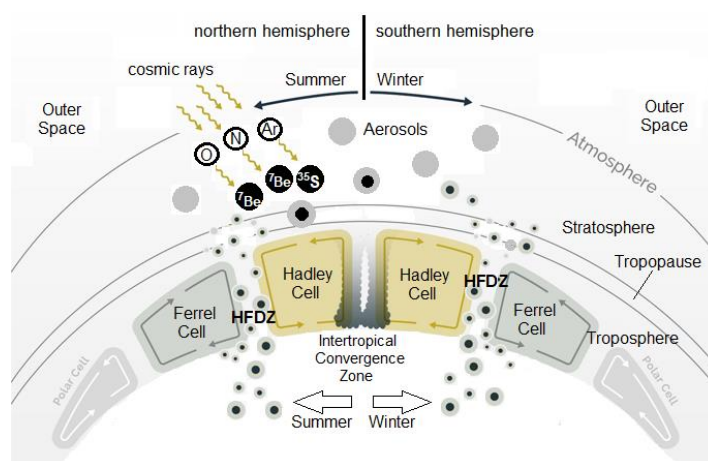
Figure 2. Schematic image displaying the creation of ^{7}Be and ^{35}S within the stratosphere by cosmic ray spallation of oxygen/nitrogen and argon, respectively, the attachment of the radionuclides onto aerosol particles and their conveyance towards the earth's surface via the HFDZ that is shifting in place with the seasons as indicated by the arrows (figure based on [32]).

Long-term ^{7}Be datasets are generally available since the parameter is recorded as a routine parameter by the Comprehensive Nuclear-Test-Ban Treaty Organization (CTBTO). A worldwide network of 80 CTBTO stations has been set up to monitor compliance with the Comprehensive Nuclear-Test-Ban Treaty. The resulting ^{7}Be datasets are freely available [10]. This makes ^{7}Be an easily attainable ^{35}S proxy.

Our study evaluated the recorded ^{35}S dataset versus a ^{7}Be time series recorded at the CTBTO station RN33, located (as sole CTBTO station in Germany) at Mount Schauinsland in the Black Forest Mountains. Due to the large spatial scale of ^{7}Be and ^{35}S production and migration processes in the atmosphere (as discussed in Section 1), the distance between the ^{7}Be and the ^{35}S recording stations (Black Forest Mountains and close to the City of Leipzig, respectively) is of only minor relevance.

2.3. Using the Aerosol Optical Depth (AOD) and ^{212}Pb in Air as Supporting Data

Besides the two large-scale atmospheric processes mentioned above in points (i) and (ii), a third reason can be given for the increase of the activity concentration of ^{35}S in the rain during the warm and dry season: (iii) a less intense ^{35}S washout from the atmosphere by rain. The less rain falls, the less intense is the washout, which results in an increase of the particle concentration in the rain when a rare precipitation event occurs. The triggering dry conditions are usually accompanied by an increased rate of resuspension of mineral dust from the earth's surface (windblown dust). The intensity of the latter effect can be evaluated based on two parameters: the aerosol optical depth (AOD) and the ^{212}Pb activity concentration in air.

The AOD indicates the attenuation of incoming solar radiation in the atmosphere by mineral dust, sea salts, volcanic ash, smoke from wildfires, pollution from factories and others. The potential sources of these attenuators indicate that the AOD is (regionally and temporarily) impacted by natural extreme events such as dust storms (with a global hotspot on the Arabian Peninsula) and/or anthropogenic activities such as land clearing fires (with a global hotspot in the Amazon Basin), or human-made air pollution (with global hotspots in northern India and eastern China). However, in Central Europe the impact of such effects on the AOD is less pronounced (although windblown atmospheric dust with a remote origin, such as northern Africa, Sahara, can be an issue). Besides, choosing the AOD wavelengths 1640 and 1020 nm for our investigation allowed focusing on the impact of mineral dust.

The AOD is continuously monitored by NASA at several AERONET sites worldwide. For our study, we used a dataset (covering the complete 12-month period of the ^{35}S sampling campaign)

recorded as daily averages at an altitude of 115 masl at the Institute for Tropospheric Research, which is located about 30 km north-east of our rain sampling station.

[212]Pb is a short-lived (half-life 12.64 h) progeny of the [232]Th decay chain and is easily detectable by gamma spectrometry due to its strong gamma line at 238.6 keV. Thorium and its progeny occur as a minor constituent of most soils on earth. Therefore, the [212]Pb activity concentration in the atmosphere can also be used as an indicator for the presence of terrestrial mineral dust (and hence for its washout by precipitation). Comparable to [7]Be, [212]Pb is also continuously monitored by the CTBTO as routine parameter. We used a 12-month [212]Pb dataset recorded (simultaneously to the [7]Be dataset) at the CTBTO station RN33 in the Black Forest Mountains for our study.

2.4. Anthropogenic [35]S Sources

Using ^{35}S as an environmental aqueous tracer with a distinct input function requires the consideration of anthropogenic ^{35}S sources and their potential impact. In nuclear facilities (i.e., power plants, reprocessing facilities, and research reactors) minor amounts of ^{35}S are continuously produced via the nuclear reactions [35]Cl(n,p)[35]S [33] and, to a lesser degree, [34]S(n,γ)[35]S [34]. The reactions are triggered by the activation of impurities in coolant liquids or solid reactor materials [35]. Furthermore, ^{35}S is in some nuclear facilities (in low activities) applied as process tracer. Both the unintentional production and the process tracer application of ^{35}S result in releases of the radionuclide from nuclear facilities, which occur with the emission of liquid effluents and/or coolant gas.

An evaluation of the impact of anthropogenic ^{35}S emissions on human health (carried out 43 years ago, [36]) concluded that not more than 4.8 MBq ^{35}S reach the overall group of worldwide adults by food ingestion per year. Due to this minor human exposure, ^{35}S does not belong to the group of radionuclides originating from anthropogenic activities systematically monitored and reported by the CTBTO or any national radiation protection organization. Hence, data on gaseous ^{35}S emissions from nuclear facilities are scarce.

A few historical data exist, though. A report by [35] summarized gaseous ^{35}S emissions from ten (west) German nuclear power plants for the 30-month period between January 1983 and June 1985. The facility-specific annual values ranged between 0.8 and 6.8 GBq/a, summing up to an annual gaseous ^{35}S emission averaged for (west) Germany of 24.7 ± 6.8 GBq/a.

We tried to compare this averaged anthropogenic release rate to the overall ^{35}S inventory of the lower atmosphere. Related atmospheric data is scarce, too. Average values of several-day periods published thirty years ago [25] revealed ^{35}S activities in atmospheric air (both attached to aerosols and as SO_2 gas) between about 0.107 and 0.225 MBq/km^3. Another available data collection includes atmospheric ^{35}S activities recorded in Germany and Norway between 1970 and 1979 [37]. These datasets revealed activities ranging between about 0.01 MBq/km^3 and 0.09 MBq/km^3 with an overall mean of 0.034 MBq/km^3. However, we consider this data less representative for the troposphere, i.e., our realm of interest, since all air samples were taken at ground level.

Based on the little available information given above, we assume for further estimations an average ^{35}S activity in the precipitation-influenced part of the troposphere over Central Europe of 0.1 MBq/km^3. For approximately assessing the impact of anthropogenic gaseous radiosulfur release on the overall ^{35}S inventory of this part of the troposphere, we roughly estimated the atmospheric ^{35}S inventory over Germany for the lower 10 km of the atmosphere (i.e., the layer that is subject to both ^{35}S removals by meteoric water and ^{35}S potential input by anthropogenic activities). If an averaged atmospheric activity of 0.1 MBq/km^3 is assumed, the atmospheric ^{35}S inventory over West Germany (with an area of about 249×10^3 km^2) sums up to about 249 GBq. Balancing the decay of this activity requires an overall ^{35}S import of 720 GBq/a. This approximate ^{35}S import estimation reveals that the anthropogenic share of it (24.7 ± 6.8 GBq/a as shown above) equals only about 3.4% of the overall ^{35}S input. Even though this estimation is very approximate, we can conclude that anthropogenic ^{35}S release is generally insignificant for the application of ^{35}S as a naturally occurring aqueous tracer.

However, as we demonstrate in our study and discuss in more detail below, the possibility of unusual anthropogenic peak releases has nevertheless to be considered.

3. Results

3.1. Cross-Evaluation of the Recorded Time Series

The following five data time series (as introduced above) were recorded simultaneously over a twelve-month period and cross-evaluated: (i) precipitation intensity, (ii) ^{35}S in the rain, (iii) ^{7}Be in air, (iv) ^{212}Pb in air, and (v) AOD at wavelengths 1640 and 1020 nm. The time series (i) and (ii) were recorded and evaluated as discrete values reflecting individual rain events; the time series (iii), (iv) and (v) were obtained as daily values and evaluated as 15-day moving averages. All datasets were collected in Germany; time series (i), (ii) and (v) in the vicinity of the city of Leipzig; time series (iii) and (iv) at CTBTO station RN33, located in the Black Forest Mountains. Due to the immense spatial scale of the investigated atmospheric processes (cf. Figure 2), the distance between the two recording stations (ca. 500 km) is of only minor relevance.

Figure 3 displays the recorded time series (i) rain intensity and (ii) ^{35}S activity concentration in the rain. The plot illustrates that samples for ^{35}S analyses were taken for all major rain events throughout the twelve-month sampling campaign. Furthermore, the figure shows that most rain events (88%) resulted in less than 6.5 mm of precipitation and could be collected quantitatively within the 200-litre HDPE container.
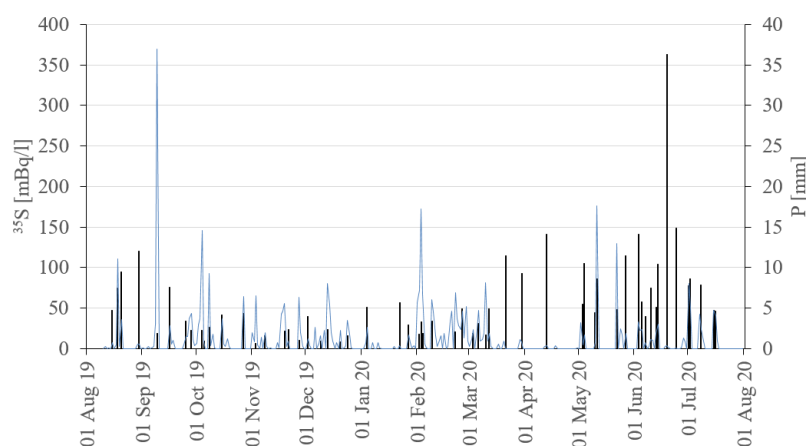

Figure 3. Complete twelve-month time series of ^{35}S activity in rain (^{35}S; black columns) and rain intensity (P, blue line).

The most intense rain event by far (37 mm) occurred on 9 September 2019 and lasted for the whole day. The related sample represents the rain that fell towards the end of the event. The detected unusually low ^{35}S activity (if compared to the two much less intense rain events that occurred before and after) illustrates the effect of dust and aerosol (and hence $^{35}SO_4$) washout by the rain during the initial hours of the event, i.e., previous to the event-specific sampling. A similar observation has been made during the major rain event on February 3rd (17.2 mm) that lasted for several hours, too. A sample taken at the beginning of the event showed a ^{35}S activity of 48 mBq/L; a sample taken towards the end of the event contained only 17 mBq/L (the mean value of 33 mBq/L was used related to this event for further evaluations).

Naturally, the recording of the ^{35}S data was bound to rain events. Due to rather dry conditions, particularly in January 2019 and between mid-March and the end of June 2020, not all periods of the twelve-month monitoring campaign could be documented satisfactorily with ^{35}S samples. Still, the ^{35}S dataset and the continuously recorded time series of ^{7}Be, ^{212}Pb and AOD (Figures 4 and 5; cf. Figure 9) reveal that all four parameters showed maxima in the second half of August 2019 and in April/May 2020. A third less distinct maximum was observed for ^{35}S and ^{7}Be in the first half of January 2020.
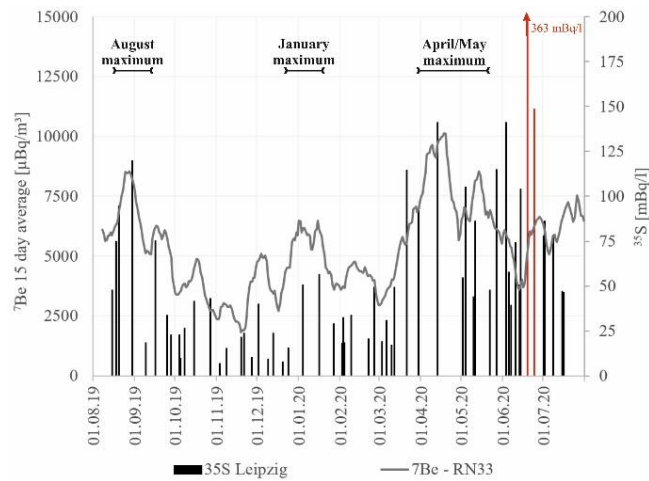
(**a**)
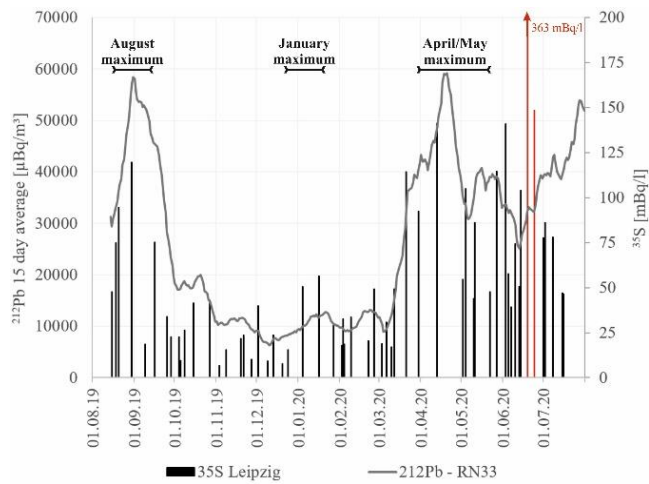
(**b**)
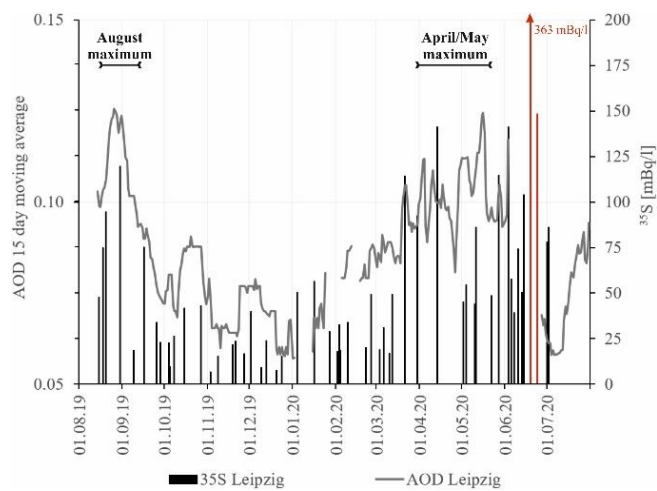
(**c**)

Figure 4. Time series (**a**) 35S/7Be, (**b**) 35S/212Pb, and (**c**) 35S/AOD (at wavelengths 1640 and 1020 nm), respectively. The 35S axis is scaled to a maximum value of 200 mBq/L, with the peak recorded in late June (max. 363 mBq/L) marked in red but not fully shown (cf. Figure 5). The unusually high AOD values recorded around this peak (max. 0.161) are not displayed either (cf. Figure 5).
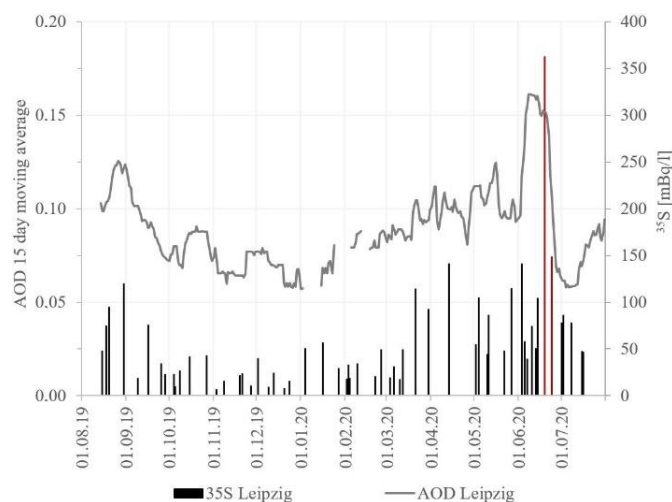
Figure 5. Complete time series ^{35}S and AOD (at wave lengths 1640 and 1020 nm).

Excluded from this summarizing evaluation is a distinct peak in ^{35}S that was recorded in the second half of June 2020. While ^{35}S showed in the previous months an average value of about 25 mBq/L and reached maximum values around 140 mBq/L, it peaked on 19th June 2020 suddenly at 363 mBq/L declining subsequently to a still considerably high 148 mBq/L (24th June 2020). Figure 4 highlight this event in red. However, in order to illustrate the previous ^{35}S data more clearly, the ^{35}S axis of the three figures is scaled to a maximum value of 200 mBq/L, i.e., the 363 mBq/L peak is not fully shown (it is fully shown in Figure 5, though). Simultaneously to the sudden ^{35}S increase, the AOD rose rather abruptly at the beginning of June. It reached a maximum value of 0.161 (8 June 2020), while the previous top values ranged around 0.125 (this AOD peak is also not shown in Figure 4c but fully displayed in Figure 5. A more detailed look at the AOD dataset reveals that the AOD was dominated by "fine mode" aerosol (90%), which is generally of anthropogenic origin (while "coarse mode" aerosol would rather indicate mineral dust). In contrast to ^{35}S and AOD, [7]Be and [212]Pb did not show significantly elevated values in the second half of June 2020.

Figure 5 displays the recorded time series ^{35}S and AOD, with the ^{35}S axis scaled to a maximum value of 400 mBq/L; i.e., including the full ^{35}S peak recorded in late June (in red) and also fully displaying the simultaneously recorded ("fine mode" aerosol, i.e., anthropogenic) AOD peak. Back trajectory analysis that allows determining the origin of the related air masses (HYSPLIT Model provided by the Air Resources Laboratory (ARL) of the US National Oceanic and Atmospheric Administration (NOAA)) suggests for the time atmospheric particle transport to the sampling site from the northwest (UK, the Netherlands). However, this general assumption is based on a set of 27 specific back trajectory ensembles (calculated by means of NOAA Hysplit Web Interface), that differ quite substantially in their lateral tracks. In fact, while the end point of all ensembles was defined to be located in Leipzig, Germany (latitude: 51.200000; longitude: 12.200000), the trajectory paths fan out (back in time) in the main to the northwest but with their specific 60 h backward direction starting points scattering over an area ranging in between Brittany in the far southwest (northern France) and the Gdańsk Bay in the far northeast (northern Poland). Hence, their informative value is (at least in the given case) limited. This limitation is, e.g., due to potential vertical mixing of air masses along the way, an uncertainty that is substantially increasing with the backtracking time.

As discussed in Section 2.2, [7]Be can be considered a direct proxy for [35]S. In general, ^{35}S in rain and [7]Be in air correlated reasonably well during the twelve-month period of the study (Figure 4). Still, the resulting correlation coefficient of the recorded twelve-month time series revealed the uncertainty of the information resulting from an evaluation of a [7]Be time series (even if supported by [212]Pb and AOD datasets) if used as proxy for [35]S (Figure 6).
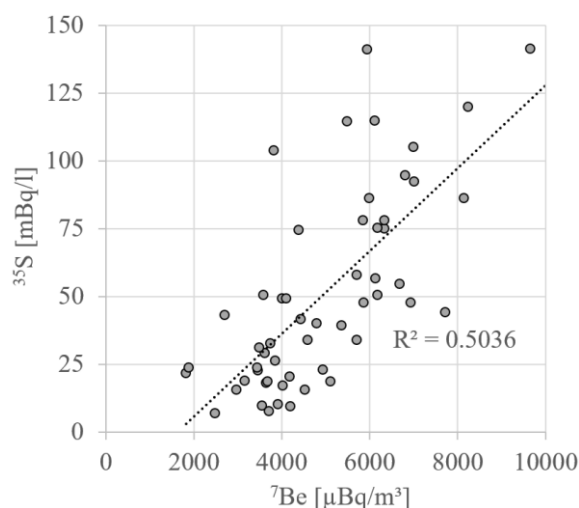
Figure 6. Correlation of ^{7}Be and ^{35}S (not considering the anomalous June 2020 peak of ^{35}S).

With the aim to improve the predictive power of the recorded ^{7}Be time series, we compared normalized values of the detected ^{35}S time series with normalized values of the ^{7}Be time series (15-day averages), i.e., we compared recorded values with the prediction parameter. Normalization of the individual values was obtained by dividing the individual activity concentrations by the overall average.

As it is shown in Figure 7, both parameters, measured and predicted, followed the same (seasonal) trend during the first 10 months of the campaign. However, from 13–16 June the comparative analysis of both parameters revealed an uncharacteristic behavior of ^{35}S.
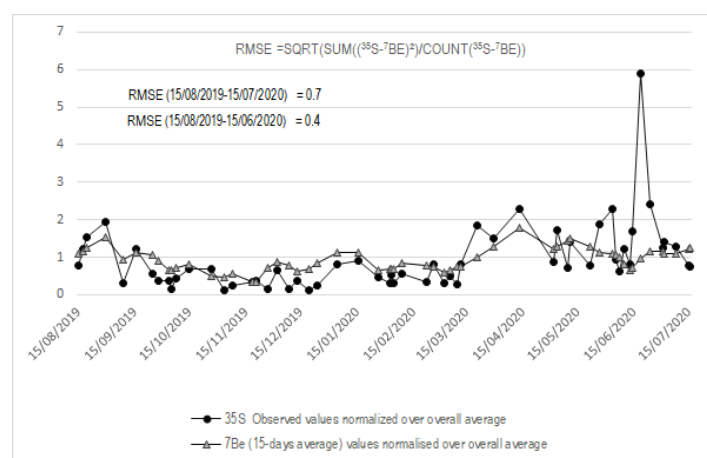

Figure 7. RMSE calculation based on normalized time series of ^{35}S and ^{7}Be.

While the calculated RMSE of the two time series between 15th August 2019 and 13th June 2020 was 0.4, the RMSE for the complete time series was 0.7. This significantly higher prediction error for the complete period of the measurement campaign was due to the anomalous peak that was observed between June and July 2020.

3.2. Natural Drivers of the Recorded Variations in ^{35}S

The simultaneous maxima of ^{35}S and ^{7}Be recorded in August 2019 and April/May 2020, respectively (Figure 4; cf. Figure 9), indicated a significantly intensified air mass exchange between higher and lower atmosphere during these times. This increased interaction is thought to be bound to two annually recurring processes that trigger an increased aerosol import from the lower stratosphere to the upper troposphere, namely (i) the cyclical altitudinal shift of the tropopause and (ii) the cyclical

lateral or latitudinal shift of the HFDZ. In 2019, the HFDZ reached central Germany around late August/September. In 2020 the approach had already occurred in April [38]. This earlier arrival of the HFDZ in 2020 was due to an early northward extension of the Hadley Cell and a corresponding stalling of the jet streams, an effect that is thought to be due to decadal climate variability or/and global warming [13].

Besides these two large-scale atmospheric processes, the less intense washout of ^{35}S and ^{7}Be from the lower atmosphere during the dry season can be named the third reason for the increase of ^{35}S in the rain and ^{7}Be in the air in August 2019 and April/May 2020. The ^{35}S and ^{7}Be datasets alone cannot evaluate the relevance of this effect. However, its substantial impact was revealed by the simultaneous significant increase of the AOD and the even more obvious increase of the ^{212}Pb activity in the air (Figure 4b,c).

The minor increase in ^{212}Pb observed in January 2020 suggests reduced particle washout as the primary reason for the less distinct maxima of ^{35}S and ^{7}Be that were observed simultaneously (AOD data is, unfortunately, missing for these days). During a five-week period starting on 26 December 2019, only minimum amounts of rainfall occurred in the wider area of the rain sampling station (overall 8 mm), thereby building up an increased aerosol concentration within the lower atmosphere.

3.3. Potential Anthropogenic Causes for Recorded Variations in ^{35}S

While the three maxima discussed in Section 3.2 can be associated to natural drivers, the significantly elevated ^{35}S values recorded in June 2020 (displayed in Figure 5) can hardly be explained with natural processes. The unusually high ^{35}S activities, which peaked on June 19th with a value of 363 mBq/L, did not reflect any increase in ^{7}Be, which excludes the stratosphere as the origin of the radiosulfur.

A potential explanation might be derived from related news that was issued in June 2020. Several public media reported at the time that elevated activities of anthropogenic radionuclides (^{134}Cs, ^{137}Cs and ^{103}Ru) had been observed in the lower atmosphere over Northern Europe in mid-June 2020, i.e., simultaneously with the ^{35}S peak in our study (e.g., reported by the CTBTO Executive Secretary Lassina Zerbo, [39]). The unusual activity concentrations had been detected at the CTBTO station RN63 (Stockholm, Sweden) (Figure 8).
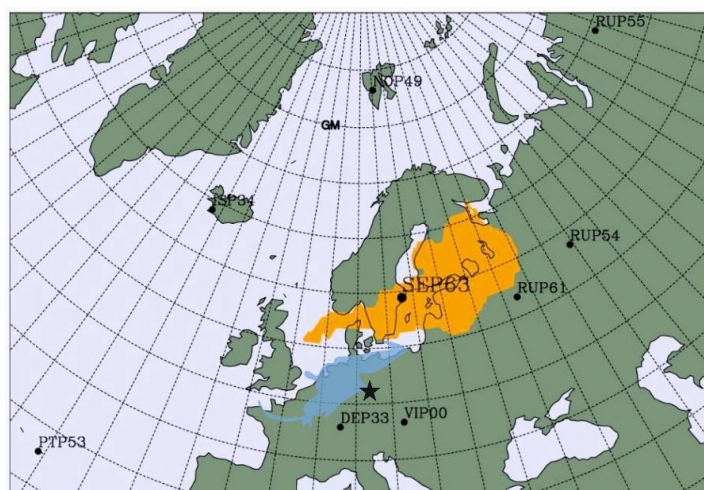

Figure 8. Map issued by the CTBTO showing in orange the possible source region of elevated atmospheric activities of anthropogenic radionuclides recorded on 22/23 June 2020; "DEP33" is indicating the location of station RN33 [39]. The black star shows the rain sampling location. Shaded in blue is the area that resulted from the modelled 60 h back trajectory ensembles discussed in Section 3.1.

Additionally to the three anthropogenic radionuclides reported by the CTBTO, our own inquiries revealed also an increase in ^{7}Be at the Swedish station RN63 (not at the German station RN33, though)

simultaneously to the ^{35}S spike observed in our study (Figure 9). Hence it could be speculated that the CTBTO observation of a minor activity release in Northern Europe points towards the same anthropogenic source responsible for the significantly elevated ^{35}S activities detected in June close to Leipzig. However, evidence for this speculation can neither be provided based on the detected nuclide pattern nor on the modelled 60 h back trajectory ensembles discussed in Section 3.1, which do not overlap with the possible source region as detected by the CTBTO (even though the overall northern direction is the same). Furthermore, we cannot explain, why this observed ^{35}S spike correlates with distinctly elevated AOD values recorded at the Leipzig AERONET site (cf. Figure 5).
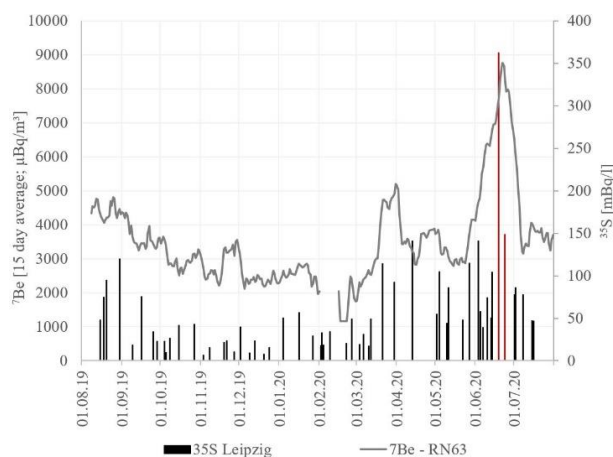

Figure 9. [35]S spike observed in Leipzig, Germany versus [7]Be spike detected at CTBTO station RN63 (Stockholm, Sweden) in June 2020.

4. Conclusions

The aims of our study were (i) to identify the drivers of the long-term variation of the ^{35}S activity concentration in rain and (ii) to evaluate the applicability of the routinely recorded [7]Be in air as proxy for setting up a ^{35}S input function that allows the use of ^{35}S as a groundwater residence time tracer. Our twelve-month sampling campaign results reveal that the time series of both ^{35}S and [7]Be show generally comparable yearly patterns with elevated values during the warm season. This pattern can be explained with two large-scale seasonal atmospheric processes: (i) the cyclical altitudinal shift of the tropopause and (ii) the cyclical latitudinal shift of the HFDZ. Additionally, the evaluated time series of [212]Pb in air and AOD revealed a noteworthy impact of (iii) reduced aerosol washout from the lower atmosphere by rain during the dry season.

Hence, if a groundwater study is to be executed to use ^{35}S as aqueous residence time tracer, we recommend the analysis of at least a few recent rain samples for their ^{35}S activity concentration and set up a ^{35}S input function based on these specific values, considering the general long-term pattern of higher ^{35}S activities in summer and lower ^{35}S activities in winter as indicated by regionally recorded datasets of [7]Be, [212]Pb and AOD. As a rough estimate we found the ^{35}S activity concentrations during the summer about three times as high as during the winter.

Furthermore, we recommend paying attention to the available time series of anthropogenic radionuclides recorded at CTBTO stations located in the wider area of the study site to become aware of any potential anthropogenic ^{35}S releases.

As the uncertainty in the input function will propagate into the calculation of the water age and age distribution patterns, it needs to be investigated further. Two key issues should be in focus in this regard: (i) dry deposition of ^{35}S and its impact on the input function and (ii) impact of rain duration and intensity on the ^{35}S activity (as shown for [22]Na by [40]).

Finally, we want to point out that each rain sample taken to set up a ^{35}S input function should represent the complete rain event. Long-lasting rains can result in a successive decrease in the ^{35}S activity concentration due to a washout of $^{35}SO_4$ containing dust and aerosols.

Author Contributions: Conceptualization: M.S.; Data curation: M.S., L.T.; Investigation: M.S., K.K.; Methodology: M.S.; L.T., I.T.; Project administration: K.K.; Writing original draft: M.S.; Writing review & editing: M.S. All authors have read and agreed to the published version of the manuscript.

Conflicts of Interest: The authors declare no conflict of interest.

References

1. Treutler, H.C.; Just, G.; Schubert, M.; Weiß, H. Radon as tracer for the determination of mean residence times of groundwater in decontamination reactors. *J. Radioanal. Nucl. Chem.* **2007**, *272*, 583–588. [CrossRef]

2. Schmidt, A.; Gibson, J.J.; Santos, I.R.; Schubert, M.; Tattrie, K.; Weiss, H. The contribution of groundwater discharge to the overall water budget of two typical Boreal lakes in Alberta/Canada estimated from a radon mass balance. *Hydrol. Earth Syst. Sci.* **2010**, *14*, 79–89. [CrossRef]

3. Petermann, E.; Gibson, J.J.; Knöller, K.; Pannier, T.; Weiß, H.; Schubert, M. Determination of groundwater discharge rates and water residence time of groundwater-fed lakes by stable isotopes of water (δ^{18}O, δ^2H) and radon (^{222}Rn) mass balances. *Hydrol. Process.* **2018**, *32*, 805–816. [CrossRef]

4. Moore, W.S.; de Oliveira, J. Determination of residence time and mixing processes of the Ubatuba, Brazil, inner shelf waters using natural Ra isotopes. *Estuar. Coast. Shelf Sci.* **2008**, *76*, 512–521. [CrossRef]

5. Rocha, C.; Wilson, J.; Scholten, J.; Schubert, M. Retention and fate of groundwater-borne Nitrogen in a coastal bay (Kinvarra Bay, Western Ireland) during summer. *Biogeochemistry* **2015**, *125*, 275–299. [CrossRef]

6. Lal, D.; Peters, B. Cosmic Ray Produced Radioactivity on the Earth. Kosmische Strahlung II/Cosmic Rays II. *Handb. Phys. Encycl. Phys.* **1962**, *9*, 551–612.

7. Koch, D.; Rind, D. ^{10}Be/^{7}Be as a tracer for atmospheric transport. *J. Geophys. Res.* **1998**, *103*, 3907–3917. [CrossRef]

8. Tilley, D.R.; Cheves, C.; Godwin, J.; Hale, G.; Hofmann, H.; Kelley, J.; Sheu, C.; Weller, H. Energy levels of light nuclei A = 5, 6, 7. *Nucl. Phys. A* **2002**, *708*, 3–163. [CrossRef]

9. Kusmierczyk-Michulec, J.; Gheddou, A.; Nikkinen, M. Influence of precipitation on ^{7}Be concentrations in air as measured by CTBTO global monitoring system. *J. Environ. Radioact.* **2015**, *144*, 140–151. [CrossRef]

10. Terzi, L.; Kalinowski, M. World-wide seasonal variation of ^{7}Be related to large-scale atmospheric circulation dynamics. *J. Environ. Radioact.* **2017**, *178–179*, 1–15. [CrossRef]

11. Landis, J.D.; Renshaw, C.E.; Kaste, J.M. Quantitative retention of atmospherically deposited elements by native vegetation is traced by the fallout radionuclides ^{7}Be and ^{210}Pb. *Environ. Sci. Technol.* **2014**, *48*, 12022–12030. [CrossRef] [PubMed]

12. Kaste, J.M.; Baskaran, M. Meteoric ^{7}Be and ^{10}Be as process tracers in the environment. In *Handbook of Environmental Geochemistry*; Baskaran, M., Ed.; Springer: Berlin/Heidelberg, Germany, 2012; pp. 61–85.

13. Terzi, L.; Wotawa, G.; Schoeppner, M.; Kalinowski, M.; Saey, P.R.J.; Steinmann, P.; Luan, L.; Staten, P.W. Radioisotopes demonstrate changes in global atmospheric circulation possibly caused by global warming. *Sci. Rep.* **2020**, *10*, 10695. [CrossRef] [PubMed]

14. Lin, M.; Thiemens, M.H. Accurate Quantification of Radiosulfur in Chemically Complex Atmospheric Samples. *Anal. Chem.* **2018**, *90*, 2884–2890. [CrossRef] [PubMed]

15. Tanaka, N.; Turekian, K.K. Use of cosmogenic ^{35}S to determine the rates of removal of atmospheric SO_2. *Nature* **1991**, *352*, 226–228. [CrossRef]

16. Urióstegui, S.H.; Bibby, R.K.; Esser, B.K.; Clark, J.F. Analytical Method for Measuring Cosmogenic ^{35}S in Natural Waters. *Anal. Chem.* **2015**, *87*, 6064–6070. [CrossRef]

17. Cho, H.-M.; Hong, Y.-L.; Kim, G. Atmospheric depositional fluxes of cosmogenic ^{35}S and ^{7}Be: Implications for the turnover rate of sulfur through the biosphere. *Atmos. Environ.* **2011**, *45*, 4230–4234. [CrossRef]

18. Hong, Y.; Kim, G. Measurement of Cosmogenic ^{35}S Activity in Rainwater and Lake Water. *Anal. Chem.* **2005**, *77*, 3390–3393. [CrossRef]

19. Osaki, S.; Tagawa, Y.; Chijiiwa, T.; Sugihara, S.; Maeda, Y. Atmospheric deposition of ^{35}S. *J. Radioanal. Nucl. Chem.* **1999**, *239*, 543–547. [CrossRef]

20. Michel, R.L.; Campbell, D.; Clow, D.; Turk, J.T. Timescales for migration of atmospherically derived sulphate through an alpine/subalpine watershed, Loch Vale, Colorado. *Water Resour. Res.* **2000**, *36*, 27–36. [CrossRef]

21. Sueker, J.K.; Turk, J.T.; Michel, R.L. Use of cosmogenic ^{35}S for comparing ages of water from three alpine/subalpine basins in the Colorado Front Range. *Geomorphology* **1999**, *27*, 61–74. [CrossRef]

22. Visser, A.; Thaw, M.; Deinhart, A.; Bibby, R.; Safeeq, M.; Conklin, M.; Esser, B.; van der Velde, Y. Cosmogenic isotopes unravel the hydrochronology and water storage dynamics of the Southern Sierra Critical Zone. *Water Resour. Res.* **2019**, *55*, 1429–1450. [CrossRef]

23. Shanley, J.B.; Mayer, B.; Mitchell, M.J.; Michel, R.L.; Bailey, S.W.; Kendall, C. Tracing sources of streamwater sulphate during snowmelt using S and O isotope ratios of sulphate and ^{35}S activity. *Biogeochemistry* **2005**, *76*, 161–185. [CrossRef]

24. Cooper, L.W.; Olsen, C.R.; Solomon, D.K.; Larsen, I.L.; Cook, R.B.; Grebmeier, J.M. Stable isotopes of oxygen and natural and fallout radionuclides used for tracing runoff during snowmelt in an Arctic watershed. *Water Resour. Res.* **1991**, *27*, 2171–2179. [CrossRef]

25. Turekian, K.K.; Tanaka, N. The use of atmospheric cosmogenic ^{35}S and [7]Be in determining depositional fluxes of SO_2. *Geophys. Res. Lett.* **1992**, *19*, 1767–1770. [CrossRef]

26. Plummer, L.N.; Busenberg, E.; Bohlke, J.K.; Nelms, D.L.; Michel, R.L. Groundwater residence times in Shenandoah National Park, Blue Ridge Mountains, Virginia, USA: A multi-tracer approach. *Chem. Geol.* **2001**, *179*, 93–111. [CrossRef]

27. Taylor, A.; Keith-Roach, M.J.; Iurian, A.R.; Mabit, L.; Blake, W.H. Temporal variability of beryllium-7 fallout in southwest UK. *J. Environ. Radioact.* **2016**, *160*, 80–86. [CrossRef]

28. Chae, J.; Kim, G. Large seasonal variations in fine aerosol precipitation rates revealed using cosmogenic [7]Be as a tracer. *Sci. Total Environ.* **2019**, *673*, 1–6. [CrossRef]

29. Schubert, M.; Kopitz, J.; Knöller, K. Improved approach for LSC detection of ^{35}S aiming at its application as tracer for short groundwater residence times. *J. Environ. Radioact.* **2019**, *208–209*, 106022. [CrossRef]

30. Schubert, M.; Kopitz, J.; Knöller, K. Low-sulphate water sample preparation for LSC detection of 35S avoiding sulphate precipitation. *J. Environ. Radioact.* **2020**, *213*, 106153. [CrossRef]

31. Delaygue, G.; Bekki, S.; Bard, E. Modelling the stratospheric budget of beryllium isotopes. *Tellus B* **2015**, *67*, 28582. [CrossRef]

32. Terzi, L.; Kalinowski, M.; Schoeppner, M.; Wotawa, G. How to predict seasonal weather and monsoons with radionuclide monitoring. *Sci. Rep. Nat. Res.* **2019**, *9*, 2729. [CrossRef]

33. Dyrssen, D.; Nyman, P.O. Slow-neutron-induced radioactivity of sea-water. *Acta Radiol.* **1955**, *43*, 421–427. [CrossRef] [PubMed]

34. Love, D.L.; Sam, D. Radiochemical determination of sodium-24 and sulfur-35 in seawater. *Anal. Chem.* **1962**, *34*, 336–340. [CrossRef]

35. Vogl, K.; Fouasnon, S.; Gesewsky, P.; Winkelmann, I. *Untersuchungen über die Emission von Phosphor-32 und Schwefel-35 Mit der Abluft aus Kernkraftwerken in der Bundesrepublik Deutschland von 1983 bis Mitte 1985—ISH Heft 84*; Bundesgesundheitsamt—Institut für Strahlenhygiene: Bonn, Germany, 1985.

36. Meyer, B. *Sulfur, Energy and Environment*, 1st ed.; Elsevier Scientific Publishing Company: Amsterdam, The Netherlands; New York, NY, USA, 1977; p. 448.

37. Kolb, W. *Aktivitätskonzentrationen von Radionukliden in der Bodennahen Luft Norddeutschlands und Nordnorwegens im Zeitraum von 1963 bis 1990*; Physikalisch-technische Bundesanstalt: Braunschweig/Berlin, Germany, 1992.

38. Terzi. 2020. Available online: https://www.derstandard.at/story/2000119021106/radioaktives-isotop-zeigt-ausmass-des-klimawandels (accessed on 21 October 2020).

39. Zerbo. 2020. Available online: https://twitter.com/SinaZerbo/status/1276559857731153921/photo/1 (accessed on 21 October 2020).

40. Kaste, J.M. Cosmogenic [22]Na as a steady-state tracer of solute transport and water age in first-order catchments. *Earth Planet. Sci. Lett.* **2016**, *456*, 78–86. [CrossRef]